

Hydrogenolysis cleavage of C_{sp2}-C_{sp3} bond over a metal-free NbOPO₄ catalyst

Received 00th January 20xx,
Accepted 00th January 20xx

DOI: 10.1039/x0xx00000x

Hao Zhou,^{a,†} Lu Chen,^{b,†} Yong Guo,^{a,*} Xiaohui Liu,^a Xin-Ping Wu,^{b,*} Xue-Qing Gong^b and Yanqin Wang^{a,*}

Ru/NbO_x catalysts, which combine the merits of facile hydrogen activation, strong binding to benzene ring and the presence of Brønsted acid sites, were well investigated toward C_{sp2}-C_{sp3} bond cleavage. Herein, we unlock the ability of bare NbO_x catalyst in the dissociation and activation of hydrogen molecule and further hydrogenolysis of the C_{sp2}-C_{sp3} model compounds including polystyrene (PS). In-situ Drift and density functional theory (DFT) calculations reveal that H₂ can be dissociated and surface hydride species can be produced over Nb₂O₅ through heterolytic and homolytic cleavages of H₂. We also find that the existence of surface oxygen vacancies plays a key role in stabilizing hydride species. Further, the NbOPO₄ catalyst not only allows the conversion of phenylcyclohexane to monocyclic compounds by cleaving C_{sp2}-C_{sp3} bond, but also enables the conversion of PS to arenes with a high selectivity. This study provides and proves for the first time, the unique ability of metal oxides (phosphates) in the hydrogenolysis of compounds and plastics containing C_{sp2}-C_{sp3} bonds.

Introduction

Sustainable fuels and chemicals have received unprecedented emphasis by the world in the context of achieving the goal of carbon neutrality. The utilization of biomass and wasted aromatic plastics, composited by monomers via C-O and/or C-C bond linkage, is an important and beneficial path to achieve this goal. To harvest fuels or chemicals from biomass or wasted plastic, the activation/scission of C-O and/or C-C bond is required.¹⁻⁵ The activation of C-O bond has been investigated widely and deeply, and therefore many catalysts have been developed to remove the excess oxygen in biomass or polyester plastics.^{2,6-8} The scission of C-C bond is also crucial as it could recover the monomers by depolymerizing biomass⁹ or plastics (e.g., polypropylene, polyethylene and polystyrene).¹⁰⁻¹² The generally higher dissociation energy of C-C bond (226-494 kJ/mol) compared to C-O bond (209-348 kJ/mol)^{13,14} brings obstacles in the depolymerization and

utilization of these resources linked by C-C bonds. Due to the importance and high challenge of C-C bond cleavage, the study on catalytic C-C bond cleavage has been attracting more and more attentions.

In fact, various strategies have emerged in breaking C-C bond. Hydrocracking, a traditional method to cleave C-C bond, was usually adopted to produce short-chain hydrocarbons in petroleum refinery. Generally, in this hydro-process for breaking C-C bond, bifunctional catalysts with both metal and acid active sites, such as Ni- or Co-modified MoS₂ or WS₂ supported on molecular sieve¹⁵ and Pt supported on Al₂O₃,¹⁶ are required. Recently, we reported a multifunctional Ru/NbOPO₄ catalyst, which could efficiently cleave C_{sp2}-C_{sp3} bond and C-O bond in one-pot conversion of lignin to monocyclic hydrocarbons.^{2,9} In the supported metal catalysts, the metals (Pt, Pd, Ru, Ni, Co) usually play a key role in activating hydrogen molecule, which is considered to be necessary in the hydro-processing.^{10-12,17-23} However, recently, Huang et al. reported that ceria with oxygen vacancies (O_v) can produce H^{δ-} species *via* the heterolytic pathway and showed good activity in hydrogenation reactions²⁴, where the oxygen vacancies played an important role in the formation and stabilisation of hydride species (CeO_v⁴⁺-H⁻).²⁵ Another study from Qu et al. also demonstrated that the solid frustrated Lewis pair was constructed by precisely controlling the surface defects of the metal oxide (CeO₂) catalyst to achieve the dissociation of hydrogen molecule with a relatively low activation energy of 0.17 eV.²⁶ In this way, metal oxide with oxygen vacancies/defects could be used as catalysts for hydrogenation reaction.

In our previous works, the catalysts of metal supported on NbO_x materials have been widely used to produce renewable chemicals and fuels from biomass or wasted plastics by

^a H. Zhou, Dr. Y. Guo*, Dr. X.H. Liu, Prof. Y. Wang*
Shanghai Key Laboratory of Functional Materials Chemistry, Research Institute of Industrial Catalysis, School of Chemistry and Molecular Engineering, East China University of Science and Technology, 130 Meilong Road, Shanghai, P. R. China
E-mail: guoyong@ecust.edu.cn; wangyanqin@ecust.edu.cn

^b L. Chen, Dr. X.-P. Wu*, Prof. X.-Q. Gong
Key Laboratory for Advanced Materials and Joint International Research Laboratory for Precision Chemistry and Molecular Engineering, Feringa Nobel Prize Scientist Joint Research Center, Centre for Computational Chemistry and Research Institute of Industrial Catalysis, School of Chemistry and Molecular Engineering, East China University of Science and Technology, 130 Meilong Road, Shanghai, 200237, P. R. China
Email: xpwu@ecust.edu.cn

[†]These two contribute equally.

* Footnotes relating to the title and/or authors should appear here.

Electronic Supplementary Information (ESI) available: [details of any supplementary information available should be included here]. See DOI: 10.1039/x0xx00000x

breaking C-C and C-O bonds.^{2,6,9,27,28} The metal sites, NbO_x species and acid sites play roles independently in the dissociation of H₂, adsorption of substrates/intermediates, and partial protonation and activation of adsorbed substrates, thus driving the efficient cleavage of C-C bond.⁹ Herein, we report the cleavage of C_{sp2}-C_{sp3} bond via hydrogenolysis over the metal-free NbOPO₄ catalyst. We demonstrate the successful cleavage of C-C bond with high efficiency under hydrogen over a metal-free catalyst by using the conversion of phenylcyclohexane to monocyclic hydrocarbons as a showcase. In addition, taking this strategy, we show that the polystyrene could be high-efficiently cut to monocyclic aromatic hydrocarbons over the metal-free catalyst. By combining diffuse reflectance infrared Fourier Transform spectra (DRIFTS) of H₂/D₂ and density functional theory (DFT) calculations, we investigated the mechanism of the heterolytic and homolytic cleavage pathways of hydrogen molecules. This finding would help the rational design and preparation of low-cost hydrogenolysis catalysts.

Results and discussion

Phenylcyclohexane is chosen as a model compound since it contains the typical C_{sp2}-C_{sp3} bond and is also one of the intermediate products in the conversion of lignin. In our previous work, we demonstrated that Ru/NbOPO₄ catalyst could break the C_{sp2}-C_{sp3} bond efficiently.⁹ Here, we used NbOPO₄ as a catalyst without metal loading to evaluate the performance of phenylcyclohexane conversion under hydrogen. The XRD pattern, N₂ sorption and Py-FRIR of NbOPO₄ are present in supporting information (Figures s1 and s2, and Table s1). Before reaction, we conducted the electron paramagnetic resonance (EPR) measurement to see if there are any oxygen vacancies in NbOPO₄ catalyst, and the result is shown in Figure 1. It clearly indicates the existence of oxygen vacancies on NbOPO₄ catalyst. Surprisingly, the catalyst of NbOPO₄ showed excellent performance in cleaving C_{sp2}-C_{sp3} bond. The yield of benzene, cyclohexane and methylcyclopentane is 46.8%, 1.8% and 37.2%, respectively, with a conversion of 99.3%, which is even comparable to the results over 2%Ru/NbOPO₄ catalyst (Table 1, entry 1&2). Considering that this reaction requires the dissociation of H₂ to active H species, we speculate some active species or sites in NbOPO₄ could activate and dissociate H₂ efficiently. As mentioned in the introduction that metal oxides with oxygen vacancies have been reported to possess the ability of dissociating H₂, here NbO_x species is thought to be able to dissociate H₂. Therefore, we exquisitely synthesized a Layered Nb₂O₅ (Nb₂O₅-L) catalyst, which is rich in oxygen vacancies and Brønsted acid sites, to verify our speculation. The XRD pattern, N₂ sorption and Py-FRIR of Nb₂O₅-L are presented in supporting information (Figures s1 and s3, and Table s1). As expected, Nb₂O₅-L performed well enough on the hydrogenolysis of phenylcyclohexane (Table 1 entry 3). Recently, TiO₂ and CeO₂ with defects (Figure S4) also have been reported to have the ability of dissociate hydrogen molecule.^{24-26,29-31} Therefore, they were taken into controlled experiments to evaluate the

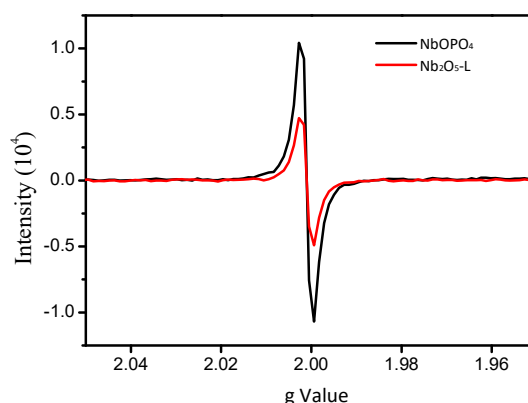


Figure 1. Electron paramagnetic resonance (EPR) spectra of NbOPO₄ and Nb₂O₅-L catalysts.

performance in the cleavage of C_{sp2}-C_{sp3} bond. Owing to the poor amounts of Brønsted acid sites in these two catalysts (Table S1), 0.05 g H₃PO₄ was added into the reaction system as the source of Brønsted acid. The conversions were only 22.1% and 3.3% over TiO₂ and CeO₂, respectively, revealing that metal oxides without metallic sites do activate H₂. The huge difference in activity between NbO_x catalyst and other metal oxides may be attributed to their different ability on the adsorption and activation of benzene ring (Figure S5).

To investigate the ability of H₂ activation on NbO_x species, the in-situ DRIFTS was conducted on Nb₂O₅-L by imputing H₂ and D₂. As shown in Figure 2a, when purging H₂ gas into the cell, the peaks at 3600-3750 cm⁻¹ and 3250-3640 cm⁻¹ appear, and these peaks are assigned to O-H free and O-H chelate stretching vibration (the blue line). It is important to note that, upon pumping H₂ gas out and introducing D₂ gas, the O-D free (2670-2740 cm⁻¹) and O-D chelate stretching vibration bands (2340-2620 cm⁻¹) increase (the green line) at the expense of the O-H bands decrease. The bands of O-H free stretching vibration at 3600-3750 cm⁻¹ decrease to a negative value, which are attributed to H-D exchange reaction of surface hydroxyl species in Nb₂O₅-L. Interestingly, in Figure 1b, the peaks at 1668 cm⁻¹, 1620 cm⁻¹, and 1233 cm⁻¹ transform into the peaks of 1642 cm⁻¹, 1498 cm⁻¹, and 1194 cm⁻¹ concomitantly when D₂ was introduced the cell. The peaks at 1194 cm⁻¹ and 1620 cm⁻¹ are ascribed to the O-D and O-H bending vibration, respectively.³² Therefore, the hydride species may emerge on the surface of catalyst due to the dissociation of H₂/D₂. Base on the discussion above, the peaks at 1668 cm⁻¹ and 1233 cm⁻¹ are suggested to be assigned to the Nb-H bond stretching (the blue line), which are consistent with the DFT results (Table S2); the different wave numbers correspond to different dissociation modes. The peaks at 1498 cm⁻¹ is suggested to be assigned to the Nb-D bond stretching (the green line); this bond corresponds to the Nb-H bond of 1668 cm⁻¹, and is produced via H-D exchange reaction. Unfortunately, the peaks of 1642 cm⁻¹ can't be properly assigned on the in-situ DRIFTS spectra. Moreover, hydride species can be detected by DRIFTS because of the presence of oxygen vacancies on the surface of the Nb₂O₅-L catalyst.

Table 1. Reaction results of conversion of phenylcyclohexane over various metal-free catalysts.^a

Entry	Catalyst	Yield (wt%)			Dicyclic (C12) ^c	Conversion (%)
		Monocyclic (C6)				
1	NbOPO ₄	46.8	1.8	37.2	5.2	99.3
2	2%Ru/NbOPO ₄	47.8	3.5	37.3	4.0	99.5
3	Nb ₂ O ₅ -L	46.3	1.8	30.9	3.6	98.3
4	TiO ₂ ^b	6.4	0.2	3.8	1.9	22.1
5	CeO ₂ ^b	0.3	-	0.3	0.6	3.3

[a] Reaction conditions: phenylcyclohexane (0.2 g), catalyst (0.1 g), H₂ 0.5 MPa, 280°C, 12h, 2 mL dodecane.

[b] Reaction conditions: phenylcyclohexane (0.2g), catalyst (0.1 g), H₃PO₄ (0.05 g), H₂ 0.5 MPa, 280°C, 12h, 2 mL dodecane.

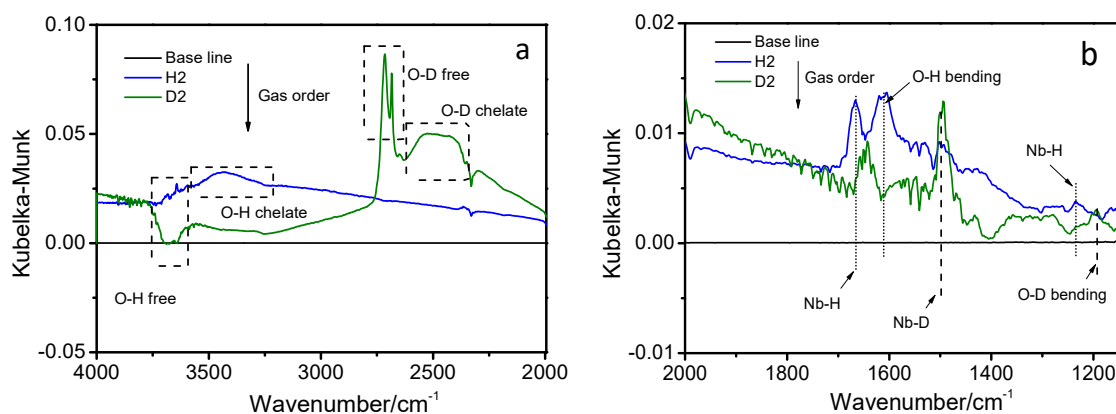
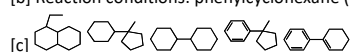


Figure 2. In situ DRIFTS spectra for Nb₂O₅-L on adsorption of hydrogen at 280°C. (a) from 4000 to 2000 cm⁻¹; (b) from 1900 to 1150 cm⁻¹.

To further understand the exceptional catalytic performance of the Nb₂O₅-L catalyst, we conducted density functional theory (DFT) calculations on the key H₂ adsorption and dissociation processes, which produce reactive hydrogen species, on the Nb₂O₅ catalyst surface. Computational details can be found in the Supporting Information. XRD pattern shows that the Nb₂O₅-L mainly exposed the (001) surface (Figure S1),³³ and oxygen vacancies were observed on the catalyst surface (see Figure 1). Therefore, we constructed pristine Nb₂O₅(001) (see Figure 3a) as well as the defective Nb₂O₅(001) with one surface oxygen vacancy (denoted as Nb₂O₅(001)-OV, see Figure 3b). The calculated results show that H₂ adsorbs weakly on the pristine Nb₂O₅(001) and Nb₂O₅(001)-OV surfaces ($E_{\text{ads}} = -0.07$ eV, see Figure 3c). It is known that H₂ dissociation on metal oxide surfaces can proceed in the homolytic way, producing two surface hydroxyls (O-H⁺), or in the heterolytic way, producing a surface hydroxyl and a hydride (H⁻). It can be seen from Figure 3c that on pristine Nb₂O₅(001) the heterolytic dissociation of H₂ is kinetically much more favorable than the homolytic one since the energy barrier of the former pathway (0.88 eV) is

significantly lower in energy than that of the latter pathway (2.75 eV), whereas the reaction energies of the two pathways are comparable to each other (former vs. latter: 0.40 vs. 0.35 eV). Interestingly, on the Nb₂O₅(001)-OV surface, heterolytic dissociation of H₂ requires an energy barrier of 0.67 eV only and is slightly endothermic by 0.01 eV, while homolytic H₂ dissociation to form two H⁺ needs to overcome a high barrier of 2.81 eV and is endothermic by 0.90 eV (see Figure 3c). Thus, the heterolytic H₂ dissociation on the Nb₂O₅(001)-OV surface is both kinetically and thermodynamically favored, which is consistent with the calculated results that on the reduced surface hydride formation is more favorable than hydroxyl formation by 0.18 eV (see Table S3 and Figure S6). Surprisingly, the homolytic H₂ dissociation to form two hydrides can readily occur at the oxygen vacancy site on the Nb₂O₅(001)-OV surface (see Figures 3c and 3d). The calculated barrier of such pathway (0.66 eV) is comparable to that of the heterolytic pathway (0.67 eV) on the same surface. Nevertheless, the homolytic dissociation product of two hydrides is 0.39 eV less stable than the heterolytic dissociation product of one hydroxyl and one hydride, which is likely due to the weak adsorption of the

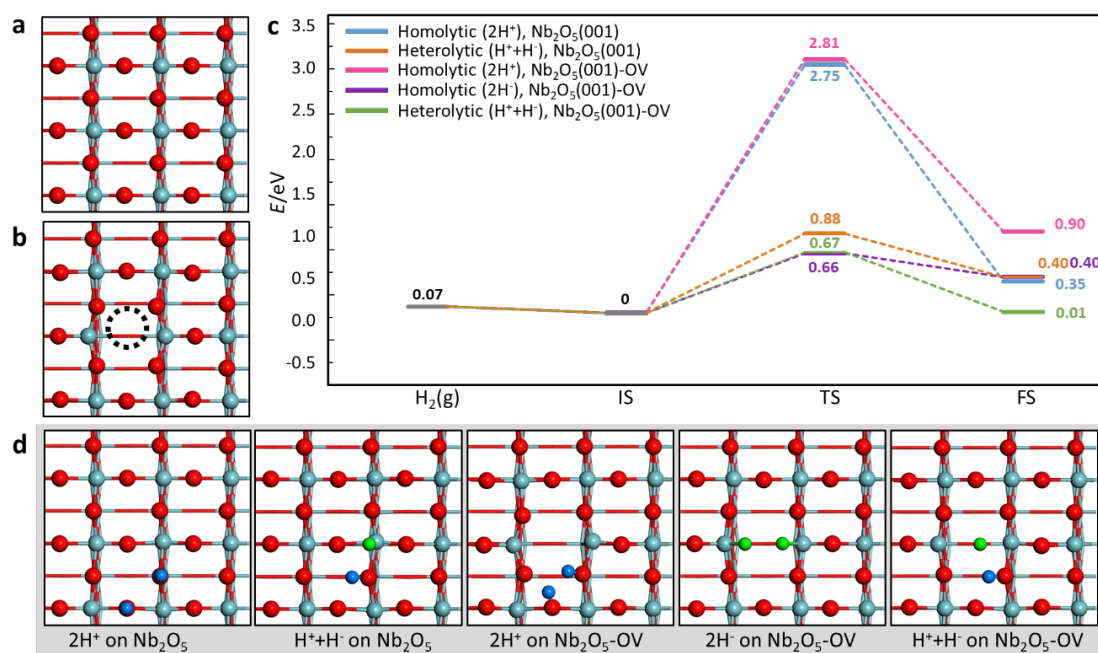


Figure 3. Optimized structures (top view) of (a) pristine $Nb_2O_5(001)$ and (b) $Nb_2O_5(001)-OV$. The black dashed circle in (b) represents the oxygen vacancy. (c) Calculated energy profiles for homolytic and heterolytic H_2 dissociations on pristine $Nb_2O_5(001)$ and $Nb_2O_5(001)-OV$ surfaces. $H_2(g)$, IS, TS, and FS represent the state with gas-phase H_2 , the initial state (surface adsorbed H_2), transition state, and final state (two hydroxyls, one hydroxyl and one hydride, or two hydrides) of H_2 dissociation. The energies of the states along the reaction pathway are referenced to the energy of IS. (d) Calculated FS structures (top view) for the various H_2 dissociation pathways. The Nb, O, proton (H^+), and hydride (H^-) are in light blue, red, blue, and green, respectively.

Table 2. Catalytic performance for the conversion of polystyrene over $NbOPO_4$ catalyst.

a

Catalyst	Products distribution (wt%)					Others in liquid ^b	Others in gas ^c	Total mass Yield (wt%)
$NbOPO_4$	27.7	5.3	3.7	4.4	7.5	1.7	1.6	51.9

[a] Reaction conditions: Polystyrene (0.2 g), catalyst (0.1 g), H_2 0.5 MPa, 280°C, 12 h, 2 mL dodecane. [b], [c] the detail was shown in Table S4.

second hydride at the oxygen vacancy site. It can be speculated that homolytic H_2 dissociation with the formation of two hydrides can be dominated on highly reduced $Nb_2O_5(001)$ surface. The above calculated results clearly suggest that surface oxygen vacancy can facilitate the dissociation of H_2 and promote the formation of hydrides on $Nb_2O_5(001)-OV$.

In order to verify the practicality of the $NbOPO_4$ catalyst, we took it as catalyst to convert polystyrene that formed solely via C-C bond (including typical $C_{sp2}-C_{sp3}$). Noteworthy, the yield of total products was 51.9% as shown in Table 2. Specifically, the yield of benzene reached to 27.7%, confirming its high activity for the cleavage of $C_{sp2}-C_{sp3}$ bond. In addition to benzene, the products via breaking other C-C bond were also obtained through the cleavage, for example, ethylbenzene, isopropylbenzene, and indane derivatives. The indane

derivatives may be attributed to the acid-catalyzed alkylation with the existence of Brønsted acid. In addition, some small amounts of products in gas phase were also detected, which were exhibited in Table S4. To explore the stability, three consecutive conversion of polystyrene were conducted with the recycled catalyst and the results are shown in Figure 4. Negligible changes on product yields are observed in the recycle tests. It is confirmed there is no change on the structure of the catalyst by X-ray diffraction (XRD) characterization (Figure S7). The stability test and XRD characterizations indicate that $NbOPO_4$ catalyst displayed excellent stability.

Conclusions

In summary, we introduced a metal-free NbOPO₄ catalyst for the hydrogenolysis reactions involving dissociation of H₂ and cleavage of C-C bond. NbOPO₄ catalyst exhibited the excellent activity to cleave C_{sp2}-C_{sp3} bond in the conversion of phenylcyclohexane and PS plastic. Through in-situ DRIFTS of H₂/D₂ adsorption and DFT calculations, we demonstrate that hydrogen could be adsorbed and dissociated over NbO_x species. Combining our previous acknowledge in C-C bond cleavage over Ru/NbOPO₄ and the discovery in this work, we conclude that the reason why metal-free NbO_x based catalysts possess so excellent ability to break the C-C bond in aromatics via hydrogenolysis is mainly because i) the NbO_x species could dissociate H₂ via Nb and O atoms to generate hydrides which could be stabilized by oxygen vacancies; and ii) the NbO_x species could strongly adsorb and activate the aromatic ring. iii) the existence of Brønsted acid sites can activate C-C bond. This study gives a deep understanding on NbO_x based catalyst and provides new mechanism for catalyst design towards cleavage of C_{sp2}-C_{sp3} bond in the hydrogen involved reactions.

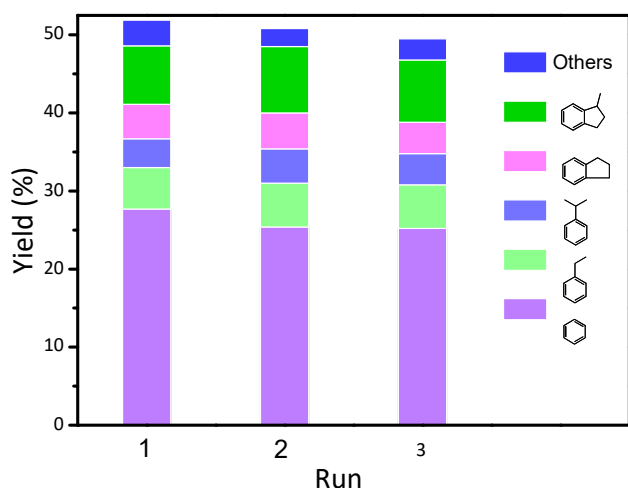


Figure 4. Recyclability test of NbOPO₄ for the conversion of polystyrene. Reaction conditions: Polystyrene (0.2 g), catalyst (0.1 g), H₂ 0.5 MPa, 280°C, 12 h, 2 mL dodecane.

Experimental Section

Preparation of NbOPO₄ and Nb₂O₅ catalyst

NbOPO₄ and Nb₂O₅-L were synthesized according to our previous works.^{6, 34} The Ru-based catalysts were prepared by the incipient wetness impregnation method with appropriate amounts of aqueous solution of RuCl₃. The obtained samples were dried at 100 °C for 12 h and then reduced in a 10% H₂/Ar flow at 400 °C for 3 h. The metal loading in catalysts was 2 wt%.

Catalyst characterizations

The powder X-ray diffraction (XRD) patterns were recorded on a Rigaku D/max-2550VB/PC diffractometer by using Cu K α radiation ($\lambda=0.15406$ nm). Nitrogen adsorption/desorption isotherms of the catalysts were measured on a Micromeritics ASAP 2020M sorption analyzer at 77K. The Brunauer-Emmett-Teller (BET) method was

used to calculate the apparent surface area. DRIFTS of hydrogen adsorption were collected with a NICOLET 670 FTIR spectrometer equipped with an MCT/A detector. Firstly, putting around 20 mg of catalyst into the chamber, the catalyst was pre-treated in flowing Ar at 280°C for 1h, followed by collecting the background spectra. Then, H₂ gas was introduced into the gas cell for 30 min, and the adsorption spectra of H₂ gas was recorded. Next, the D₂ gas was introduced instead of H₂ gas, and the adsorption spectra of D₂ gas was recorded. All spectra were collected after subtracting the background with a resolution of 4 cm⁻¹ and an accumulation of 32 scans.

Catalytic reactions

Stainless-steel autoclave reactor (50 ml) was chosen to carry out the catalytic experiment with 2 ml dodecane as solvent. In a typical run, the feedstock (0.2 g) and catalyst (0.1 g) were added into the reactor, after sealing the reactor, it was purged three times with N₂ and charged with 0.5 MPa H₂. Then it was stirred for 12 h at a magnetic stirring speed of 700 rpm at 280°C. At the end of the reaction, it was cooled to room temperature in ice water, and the organic phase was separated and analysed by GC-MS (Agilent 7890A) and quantitatively analysed by GC (Agilent 7890B) with a flame ionization detector, both equipped with HP-5 capillary columns. Pentadecane was used as an internal standard for the quantification of the liquid products. The product yields were calculated by using the equation: (mass of product) / (mass of feedstock input) \times 100%.

Conflicts of interest

There are no conflicts to declare

Acknowledgements

This work was supported financially by the NSFC of China (No. 21832002, 21808063, 21808043, 21872050, 22003016), and the Science and Technology Commission of Shanghai Municipality (10dz2220500).

Notes and references

- Z. Sun, G. Bottari, A. Afanasenko, M. C. A. Stuart, P. J. Deuss, B. Fridrich and K. Barta, *Nat. Catal.*, 2018, **1**, 82-92.
- Y. Jing, Y. Wang, S. Furukawa, J. Xia, C. Sun, M. J. Hulse, H. Wang, Y. Guo, X. Liu and N. Yan, *Angew. Chem. Int. Ed.*, 2021, **60**, 5527-5535.
- W. Schutyser, T. Renders, S. Van den Bosch, S.-F. Koelewijn, G. Beckham and B. F. Sels, *Chem. Soc. Rev.*, 2018, **47**, 852-908.
- M. Besson, P. Gallezot and C. Pinel, *Chem. Rev.*, 2014, **114**, 1827-1870.
- B. Sharma, Y. Goswami, S. Sharma and S. Shekhar, *Renew. Sust. Energ. Rev.*, 2021, **146**.
- Q. N. Xia, Q. Cuan, X. H. Liu, X. Q. Gong, G. Z. Lu and Y. Q. Wang, *Angew. Chem. Int. Ed.*, 2014, **53**, 9755-9760.

7. X. Wang, M. Arai, Q. Wu, C. Zhang and F. Zhao, *Green Chem.*, 2020, **22**, 8140-8168.
8. A. Shivhare, A. Kumar and R. Srivastava, *Green Chem.*, 2021, **23**, 3818-3841.
9. L. Dong, L. Lin, X. Han, X. Si, X. Liu, Y. Guo, F. Lu, S. Rudić, S. F. Parker, S. Yang and Y. Wang, *Chem*, 2019, **5**, 1521-1536.
10. J. E. Rorrer, G. T. Beckham and Y. Román-Leshkov, *JACS Au*, 2020, **1**, 8-12.
11. S. B. Liu, P. A. Kots, B. C. Vance, A. Danielson and D. G. Vlachos, *Sci. Adv.*, 2021, **7**.
12. M. Utami, K. Wijaya and W. Trisunaryanti, *Mater. Chem. Phys.*, 2018, **213**, 548-555.
13. R. Rinaldi, R. Jastrzebski, M. T. Clough, J. Ralph, M. Kennema, P. C. Bruijninx and B. M. Weckhuysen, *Angew. Chem. Int. Ed.*, 2016, **55**, 8164-8215.
14. M. Wang and F. Wang, *Adv. Mater.*, 2019, **31**, e1901866.
15. J. I. Mirena, J. W. Thybaut, G. B. Marin, J. A. Martens and V. V. Galvita, *Ind. Eng. Chem. Res.*, 2021, **60**, 6357-6378.
16. F. Zhang, M. Zeng, R. D. Yappert, J. Sun, Y. H. Lee, A. M. LaPointe, B. Peters, M. M. Abu-Omar and S. L. Scott, *Science*, 2020, **370**, 437-441.
17. S. Wang, K. Zhang, H. Li, L. P. Xiao and G. Song, *Nat. Commun.*, 2021, **12**, 416.
18. M. A. Hossain, T. K. Phung, M. S. Rahaman, S. Tulaphol, J. B. Jasinski and N. Sathitsuksanoh, *Appl. Catal. A: Gen.*, 2019, **582**.
19. R. C. Nelson, B. Baek, P. Ruiz, B. Goundie, A. Brooks, M. C. Wheeler, B. G. Frederick, L. C. Grabow and R. N. Austin, *ACS Catal.*, 2015, **5**, 6509-6523.
20. D. Wu, Q. Wang, O. V. Safonova, D. V. Peron, W. Zhou, Z. Yan, M. Marinova, A. Y. Khodakov and V. V. Ordomsky, *Angew. Chem. Int. Ed.*, 2021, **60**, 12513-12523.
21. J. Lu, M. Wang, X. Zhang, A. Heyden and F. Wang, *ACS Catal.*, 2016, **6**, 5589-5598.
22. H. Huang, R. Zong and H. Li, *ACS Sustainable Chem. Eng.*, 2020, **8**, 15998-16009.
23. S. Li, M. Dong, J. Yang, X. Cheng, X. Shen, S. Liu, Z. Q. Wang, X. Q. Gong, H. Liu and B. Han, *Nat. Commun.*, 2021, **12**, 584.
24. Z. Zhang, Z.-Q. Wang, Z. Li, W.-B. Zheng, L. Fan, J. Zhang, Y.-M. Hu, M.-F. Luo, X.-P. Wu, X.-Q. Gong, W. Huang and J.-Q. Lu, *ACS Catal.* 2020, **10**, 14560-14566.
25. Z. Li, K. Werner, L. Chen, A. Jia, K. Qian, J. Q. Zhong, R. You, L. Wu, L. Zhang, H. Pan, X.-P. Wu, X.-Q. Gong, S. Shaikhutdinov, W. Huang and H. J. Freund, *Chem. Eur. J.*, 2021, **27**, 5268-5276.
26. S. Zhang, Z. Q. Huang, Y. Ma, W. Gao, J. Li, F. Cao, L. Li, C. R. Chang and Y. Qu, *Nat. Commun.*, 2017, **8**, 15266.
27. Q. Xia, Z. Chen, Y. Shao, X. Gong, H. Wang, X. Liu, S. F. Parker, X. Han, S. Yang and Y. Wang, *Nat. Commun.*, 2016, **7**, 11162.
28. L. Dong, J. Xia, Y. Guo, X. Liu, H. Wang and Y. Wang, *J. Catal.*, 2021, **394**, 94-103.
29. Z. Wu, F. Xiong, Z. Wang and W. Huang, *Chin. Chem. Lett.* 2018, **29**, 752-756.
30. W. Wan, X. Nie, M. J. Janik, C. Song and X. Guo, *J. Phys. Chem. C*, 2018, **122**, 17895-17916.
31. S. Tosoni and G. Pacchioni, *J. Phys. Chem. C*, 2018, **123**, 7952-7960.
32. P. Liu, Y. Zhao, R. Qin, S. Mo, G. Chen, L. Gu, D. M. Chevrier, P. Zhang, Q. Guo, D. Zang, B. Wu, G. Fu and N. Zheng, *Science*, 2016, **352**, 797-801.
33. Y. Xin, L. Dong, Y. Guo, X. Liu, Y. Hu and Y. Wang, *J. Catal.*, 2019, **375**, 202-212.
34. Y. Zhang, J. Wang, J. Ren, X. Liu, X. Li, Y. Xia, G. Lu and Y. Wang, *Catal. Sci. Technol.*, 2012, **2**.